nature photonics

LETTERS

https://doi.org/10.1038/s41566-020-0675-0

Check for updates

Generalized Kramers–Kronig receiver for coherent terahertz communications

T. Harter[1,2,5], C. Füllner[1,5], J. N. Kemal[1], S. Ummethala[1,2], J. L. Steinmann[3], M. Brosi[3], J. L. Hesler[4], E. Bründermann[3], A.-S. Müller[3], W. Freude[1], S. Randel[1] and C. Koos[1,2] ✉

Modern communication systems rely on efficient quadrature amplitude modulation formats that encode information on both the amplitude and phase of an electromagnetic carrier. Coherent detection of such signals typically requires complex receivers that contain a continuous-wave local oscillator as a phase reference and a mixer circuit for spectral down-conversion. In optical communications, the so-called Kramers–Kronig scheme has been demonstrated to simplify the receiver, reducing the hardware to a single photodiode[1–3]. In this approach, a local-oscillator tone is transmitted along with the signal, and the amplitude and phase of the complex signal envelope are digitally reconstructed from the photocurrent by exploiting their Kramers–Kronig-type relation[4–6]. Here, we transfer the Kramers–Kronig scheme to high-speed wireless communications at terahertz carrier frequencies. To this end, we generalize the approach to account for non-quadratic receiver characteristics and employ a Schottky-barrier diode as a nonlinear receiver element. Using 16-state quadrature amplitude modulation, we transmit a net data rate of 115 Gbit s^{-1} at a carrier frequency of 0.3 THz over a distance of 110 m.

Future mobile communication networks will crucially rely on wireless backbone networks with high-speed point-to-point links[7,8]. To offer data rates of 100 Gbit s^{-1} or more, these links will have to exploit unoccupied spectral resources at carrier frequencies[7,9–14] above 0.1 THz, where frequency windows of low atmospheric attenuation enable transmission over practically relevant distances of a few hundred metres[15,16]. To generate the underlying terahertz data signals, coherent down-conversion of optical waveforms in high-speed photodiodes has been demonstrated as a particularly promising approach[7,10–14,17–19]. This concept opens a simple path towards quadrature amplitude modulation (QAM) formats that offer fast transmission at high spectral efficiencies. Coherent reception of these signals, however, largely relies on relatively complex terahertz circuits, which comprise, for example, high-speed mixers along with terahertz local oscillators (LOs). These circuits are costly and often represent the bandwidth bottleneck of the transmission link[10].

Here we demonstrate a greatly simplified coherent receiver scheme for terahertz data signals that relies on a simple envelope detector and subsequent digital signal processing (DSP)[20]. The scheme allows reconstruction of the phase of the terahertz waveform from the measured envelope and relies on a generalization of the so-called Kramers–Kronig (KK) receiver in optical communications[1,2]. In our experiments, we use a high-speed Schottky-barrier diode (SBD) as a broadband and compact envelope detector. In contrast to a conventional photodetector used in optical communications, the SBD features non-quadratic rectification characteristics, which must be accounted for in our generalized KK algorithm. We demonstrate transmission of quadrature phase-shift keying (QPSK) and 16-state QAM (16QAM) signals at a carrier frequency $f_{\mathrm{THz}} = 0.3$ THz over a distance of 110 m, achieving line rates of up to 132 Gbit s^{-1} and net data rates of up to 115 Gbit s^{-1} after subtraction of the error-correction overhead. To the best of our knowledge, this is the first experiment using an envelope detector and subsequent KK processing in wireless communications, leading to the highest data rate so far demonstrated for terahertz transmission over distances of more than 100 m. Our simplified terahertz receiver perfectly complements optoelectronic wireless transmitters[7,10–14,17–19], thereby paving the way towards terahertz transmission systems that do not need any electronic terahertz circuits for signal generation and detection.

The vision of a future wireless backbone network is shown in Fig. 1. Small radio cells[21,22] with coverage of only a few tens of metres enable frequency reuse and guarantee broadband service for large numbers of terminal devices. The various cells are connected by high-capacity terahertz backhaul links in a mesh configuration, thus increasing network resilience and flexibility while decreasing installation costs in comparison with fibre-based connections. With expected per-cell peak data rates of 20 Gbit s^{-1} in fifth-generation (5G) networks[23] and 100 Gbit s^{-1} in sixth-generation networks[24], wireless terahertz backhaul links will have to offer transmission capacities of 100 Gbit s^{-1} or more to allow for flexible traffic aggregation. The inset of Fig. 1 shows a schematic of the terahertz link using a KK receiver scheme. The KK approach greatly reduces the complexity of the receiver hardware, which consists of only an amplifier and an SBD and does not require any technically complex terahertz LOs and mixer circuits.

On a fundamental level, KK processing[1] relies on the fact that the real and imaginary parts of an analytic time-domain signal represent a Hilbert transform pair. This relationship can be translated into an equivalent relationship that allows the phase of a complex signal to be retrieved once its amplitude has been measured (see Methods). For the KK-based reception described here, the terahertz signal incident at the receiver can be described as

$$u_{\mathrm{THz}}(t) = \Re\left\{\underline{U}(t)\mathrm{e}^{j2\pi f_{\mathrm{THz}}t}\right\}, \qquad (1)$$

where j is the imaginary unit, $\Re\{.\}$ denotes the real part, and where the complex envelope as a function of time t, $\underline{U}(t)$, consists of a

[1]Institute of Photonics and Quantum Electronics (IPQ), Karlsruhe Institute of Technology (KIT), Karlsruhe, Germany. [2]Institute of Microstructure Technology (IMT), Karlsruhe Institute of Technology (KIT), Karlsruhe, Germany. [3]Institute for Beam Physics and Technology (IBPT), Karlsruhe Institute of Technology (KIT), Karlsruhe, Germany. [4]Virginia Diodes Inc. (VDI), Charlottesville, VA, USA. [5]These authors contributed equally: T. Harter, C. Füllner. ✉e-mail: christian.koos@kit.edu

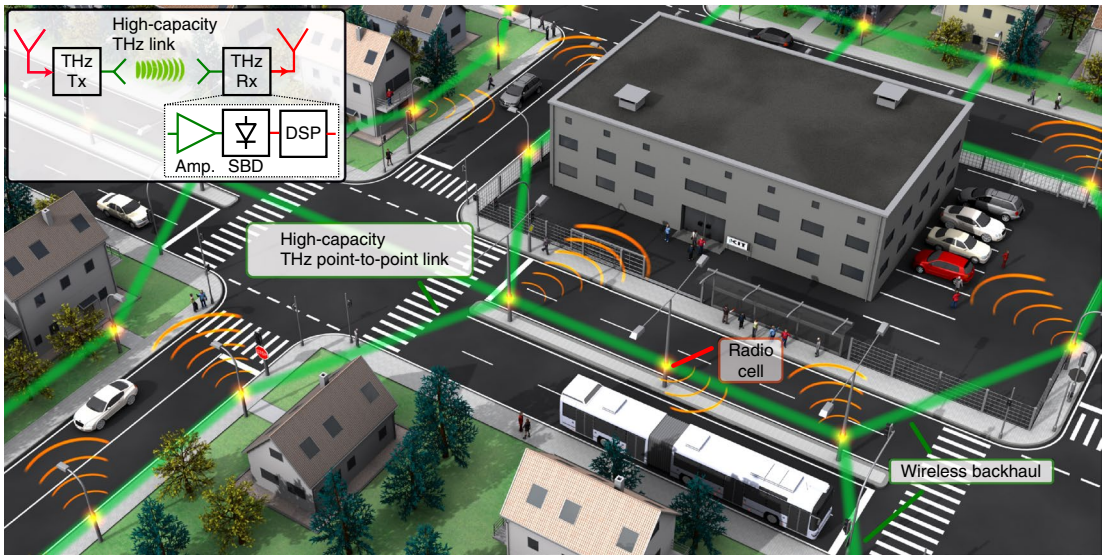

Fig. 1 | Vision of a future wireless backbone network. High-capacity terahertz line-of-sight links connect small radio cells with coverage of only a few tens of metres. Each of these cells locally guarantees ultra-broadband wireless services. The wireless connections allow flexible and efficient installation without the need for deploying optical fibres or changing fibre installations if reconfigurations are required. The inset shows a schematic of a terahertz link based on a KK-type receiver. This scheme greatly reduces the complexity of the receiver hardware by replacing technically complex terahertz LOs and mixer circuits with a simple SBD. Antennas and waveguides for terahertz signals are coloured in green, whereas red is used for radio-frequency components. Tx, transmitter; Rx, receiver; Amp., amplifier.

strong real-valued constant part U_0 and an analytic data signal $\underline{U}_s(t)$ with a single-sided power spectrum

$$\underline{U}(t) = U_0 + \underline{U}_s(t) = |\underline{U}(t)|e^{j\Phi(t)}. \quad (2)$$

To ensure correct reconstruction of the phase $\Phi(t)$ from the measured amplitude $|\underline{U}(t)|$, $\underline{U}(t)$ must be a minimum-phase signal in the time domain, which is ensured by[1]

$$|\underline{U}_s(t)| < U_0 \ \forall\ t. \quad (3)$$

The phase can then be reconstructed by a KK-type relation:

$$\Phi(t) = \frac{1}{\pi}\mathcal{P}\int_{-\infty}^{\infty}\frac{\ln(|\underline{U}(\tau)|)}{t-\tau}\mathrm{d}\tau, \quad (4)$$

where $\mathcal{P}$ denotes the Cauchy principal value of the otherwise undefined improper integral. A more detailed derivation can be found in Methods.

In optical communications, a photodiode is commonly used as an envelope detector for KK reception. Since the photocurrent is proportional to the incident optical power, the magnitude of the optical amplitude can be digitally reconstructed from the electrical signal by a simple square-root operation. In contrast to this, SBDs feature complex rectification characteristics, thus requiring a generalization of the KK-based signal reconstruction algorithm. To this end, we assume that the relationship between the amplitude of the terahertz signal at the SBD receiver input $|\underline{U}(t)|$ and the current $i(t)$ at the output can be described by a bijective function g

$$i(t) = g(|\underline{U}(t)|), \quad (5)$$

(see Supplementary Section 2). The amplitude can then be reconstructed by applying the inverse function $g^{-1}(i)$ to the measured output current, and the phase $\Phi(t)$ can be found by replacing $\ln(|\underline{U}(t)|)$ in equation (4) with the generalized expression $\ln(g^{-1}(i))$:

$$\Phi(t) = \frac{1}{\pi}\mathcal{P}\int_{-\infty}^{\infty}\frac{\ln(g^{-1}(i(\tau)))}{t-\tau}\mathrm{d}\tau. \quad (6)$$

In contrast to square-law photodetectors, the exact rectification characteristics of SBDs depend crucially on the operating point as well as on the peripheral terahertz and baseband circuits and are hence hard to describe analytically. We therefore express $g^{-1}(i)$ as a power series with $N+1$ initially unknown coefficients a_n

$$|\underline{U}_R| = g^{-1}(i) = \sum_{n=0}^{N} a_n i^n. \quad (7)$$

In this relation, $|\underline{U}_R|$ denotes the terahertz voltage amplitude that is reconstructed from a measured current i at the SBD output. The coefficients a_n have to be determined from measured data. To this end, we use test signals with known amplitudes $|\underline{U}(t)|$ and measure the associated current $i(t)$ at discrete times t_m, with $m = 1,2,\ldots M$ and $M \gg N$. The coefficients a_n are obtained from a least-squares fit of the polynomial function $|\underline{U}_R(t_m)| = g^{-1}(i(t_m))$, given by equation (7), to the known data set $|\underline{U}(t_m)|$ (Supplementary Section 3). The result is shown in Fig. 2, together with the square-root characteristics that would be used in conventional KK processing of optical signals. While the square-root characteristics can be used as an approximation for small signal amplitudes, the generalized approach accounts for the actual behaviour of the SBD receiver over a large range of signal levels. In addition, the generalized function comprises an offset $a_0 \neq 0$ that assigns a zero output current $i = 0$ to a non-zero terahertz amplitude $|\underline{U}_R| = g^{-1}(0)$ (Supplementary Section 3). This offset avoids small values of the reconstructed terahertz amplitude, which would otherwise require artificial clipping[25] of the signals at low reconstructed voltages to mitigate large uncertainties in the phase reconstruction according to equation (4) due to

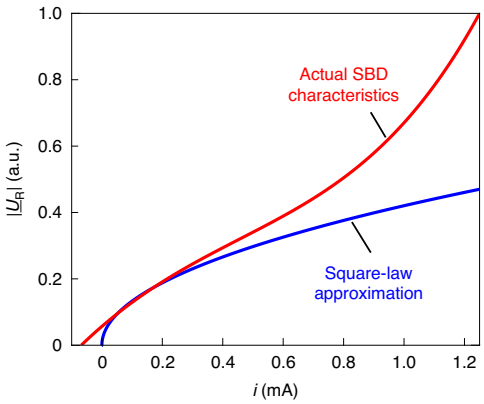

Fig. 2 | SBD receiver characteristics. The SBD rectifies the incident terahertz signal, leading to an output current i that depends on the voltage amplitude $|\underline{U}|$. We describe the actual receiver characteristics $|\underline{U}_R| = g^{-1}(i)$ (red) by a power-series approximation according to equation (7). The coefficients a_n are determined from measured test signals (Supplementary Section 3). As a reference, we show the square-root relationship (blue) that is assumed in conventional KK processing and that leads to a relationship of the form $|\underline{U}_R| \propto \sqrt{i}$. The generalized approach describes the actual behaviour of the SBD receiver for all signal levels, whereas the square-root characteristics can be used as an approximation for small signal levels only. The terahertz amplitude $|\underline{U}_R|$ is indicated in arbitrary units (a.u.), normalized to a maximum value of 1. Note that the generalized function comprises an offset $a_0 \neq 0$ that assigns a non-zero terahertz amplitude $|\underline{U}_R| = g^{-1}(0)$ to a zero output current $i = 0$, thereby effectively clipping small signal amplitudes[25] (Supplementary Section 3).

the singularity of $\ln(|\underline{U}_R|)$ at $|\underline{U}_R| = 0$. Note that the measurement data used for the least-squares fit were obtained from an SBD in combination with a terahertz amplifier at its input. The extracted receiver characteristics $g^{-1}(i)$ hence not only account for the SBD but can also compensate the saturation behaviour of the terahertz amplifier. More details on the characterization of the SBD and the terahertz amplifier can be found in Supplementary Sections 3 and 4. Note also that the non-quadratic characteristics of the SBD can broaden the received signal spectrum and might increase the bandwidth requirements of the receiver circuits. This effect, however, is not very prominent (Supplementary Section 5).

To demonstrate the viability of generalized KK processing, we perform wireless transmission experiments at $f_{THz} = 0.3$ THz. Figure 3 depicts a simplified sketch of the experimental set-up (for a comprehensive description, see Supplementary Section 1). At the transmitter, the terahertz signal is generated by frequency down-conversion of an optical signal via photomixing. An arbitrary-waveform generator (AWG) is used to drive an electro-optic in-phase/quadrature-phase (IQ) modulator, which encodes data signals with bandwidth B on an optical carrier with frequency f_0. The optical data signal is combined with two continuous-wave tones at optical frequencies f_1 and f_2 and then fed to a high-speed uni-travelling-carrier photodiode (UTC-PD)[26] for photomixing. The overall optical power entering the UTC-PD is between 10 dBm and 14 dBm, depending on the desired terahertz power (P_{THz}). The optical spectrum at the input of the photodiode is shown in the bottom left inset of Fig. 3. The first optical continuous-wave tone, at frequency f_1, serves as an LO for KK reception, whereas the second continuous-wave tone, at frequency f_2, is used for down-converting the data signal and the LO tone to $f_{THz} = f_1 - f_2 = 0.3$ THz. The LO tone at f_1 is placed at the edge of the data signal spectrum, and the data signal can hence be represented by a complex analytic signal $\underline{U}_s(t)$ with respect to the terahertz carrier frequency. The total voltage envelope is then given by $\underline{U}(t) = U_0 + \underline{U}_s(t)$, see equation (2), where U_0 denotes the LO amplitude generated by the optical tone at f_1. For distortion-free KK processing, the chosen power of the continuous-wave LO tone has to be large enough to guarantee that the resulting $\underline{U}(t)$ fulfils the minimum-phase condition according to equation (3). Note that in contrast to conventional SBD-based self-coherent transmission[27,28], generalized KK processing avoids unused guard bands between the LO tone and the payload signal, which would occupy at least half of the available transmission bandwidth.

After photomixing, the terahertz signals are radiated into free space by a horn antenna. A subsequent polytetrafluoroethylene lens collimates the beam. After a transmission distance of 110 m, the terahertz signal is collected by a second lens and another horn antenna. The transmission loss of the free-space section amounts to 17 dB and is (over-)compensated by a low-noise amplifier with 25 dB gain. The SBD is connected to the output of the amplifier (bottom right inset of Fig. 3), and a real-time oscilloscope with 80 GHz bandwidth is used to record the output current $i(t)$. After data acquisition, we apply the generalized KK algorithm, followed by blind coherent DSP (see Methods). This leads to the constellation diagrams shown in the right inset of Fig. 3. All experiments are performed indoors under laboratory conditions. For outdoor operation, additional attenuation due to adverse weather conditions must be considered. At heavy rain of, for example, 40 mm h^{-1}, the path loss of a 110-m-long link operated at a carrier frequency of 0.3 THz would increase by approximately 2.4 dB (Supplementary Section 10). This attenuation can be easily compensated by, for example, an additional terahertz amplifier at the transmitter.

In our experiments, we explore QPSK, 16QAM and 32-state QAM (32QAM) as modulation formats. The results of QPSK and 16QAM are summarized in Figs. 4 and 5, respectively. We use generalized KK processing as described above and compare it with the results obtained by conventional KK processing when assuming a square-root relationship between the SBD output current and the terahertz amplitude. We also consider evaluation assuming heterodyne reception without any KK processing. In this case, down-conversion leads to an LO-signal mixing product that is impaired by the nonlinear mixing of the signal with itself (see Methods). In a first series of experiments, we analyse the influence of the optical carrier-to-signal power ratio (CSPR) on the signal quality for QPSK modulation (Fig. 4a). The CSPR, expressed in decibels, is given by the power ratio between the LO tone and the data signal

$$\mathrm{CSPR} = 10\log\left(\frac{|U_0|^2}{\overline{|U_s(t)|^2}}\right), \tag{8}$$

where $\overline{|U_s(t)|^2}$ denotes the time average of the squared signal voltage. When changing the CSPR, the sum of carrier and signal power is kept constant at $P_{THz} = 260\,\mu$W, measured at the input port of the SBD. For QPSK signalling, the high quality of the received constellation diagram leads to a small number of errors for the 3×10^5 evaluated symbols, and the measured bit error ratio (BER) does not represent a reliable estimate for the bit error probability. We therefore use the error vector magnitude (EVM) as a quality metric[29,30] (see Methods). We find an optimum CSPR of approximately 6–7 dB for both generalized and conventional KK processing as well as for heterodyne reception without KK processing. For smaller CSPRs, the EVM obtained from KK processing increases because, for a given overall terahertz power P_{THz}, the LO magnitude becomes smaller, and the minimum-phase condition according to equation (3) is violated. For heterodyne reception without KK processing, the nonlinear interaction of the signal with itself can no longer be neglected if the CSPR is too small, thus impairing the signal quality.

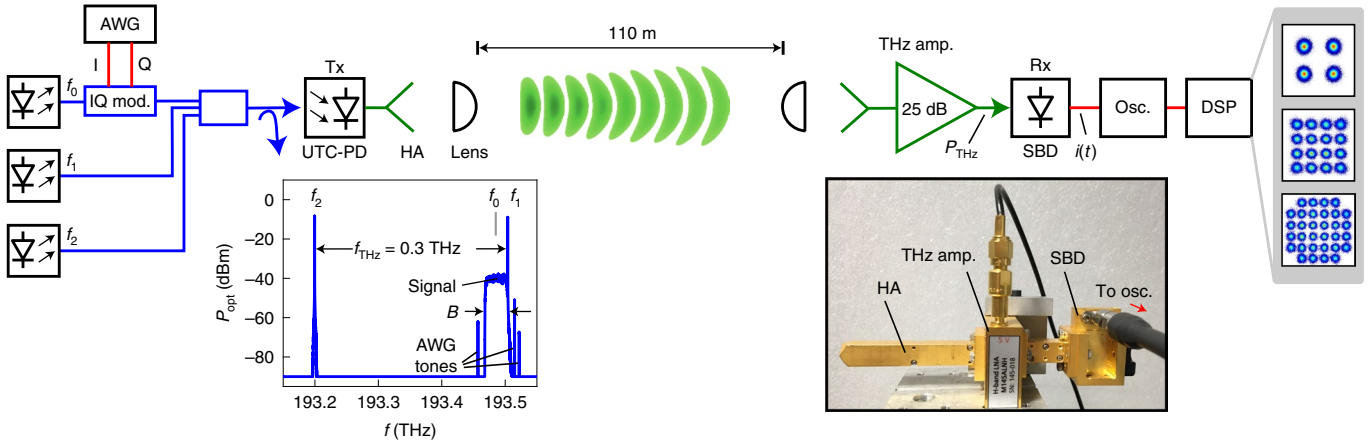

Fig. 3 | Experimental set-up. An optical data signal centred at frequency f_0 is generated by an IQ modulator ('IQ mod.') driven by an AWG. The optical data signal is then combined with two continuous-wave tones at f_1 and f_2. The tone at f_1 is placed at the edge of the data spectrum and will eventually act as an LO for KK reception, whereas the tone at f_2 serves as a reference tone for down-converting the data signal to $f_{THz}=f_1-f_2=0.3$ THz by photomixing in a high-speed UTC-PD. At the output of the UTC-PD, the terahertz signals are radiated into free space by a horn antenna ('HA') and a subsequent polytetrafluoroethylene collimation lens. After a transmission distance of 110 m, the terahertz signal is received by a second lens and another horn antenna and fed to a terahertz amplifier providing a 25 dB gain. The SBD is connected to the output of the amplifier, and a real-time oscilloscope ('Osc.') is used to capture the output current of the SBD for further offline processing ('DSP'). Bottom left inset: Corresponding optical spectrum (resolution bandwidth 180 MHz) recorded after a monitoring tap. The optical spectrum also exhibits spurious tones generated by the AWG ('AWG tones'). Bottom right inset: photograph of the receiver, including the horn antenna, the terahertz amplifier and the SBD. Right inset, top to bottom: exemplary constellation diagrams for QPSK, 16QAM and 32QAM at symbol rates of 30 GBd, 15 GBd and 5 GBd, respectively.

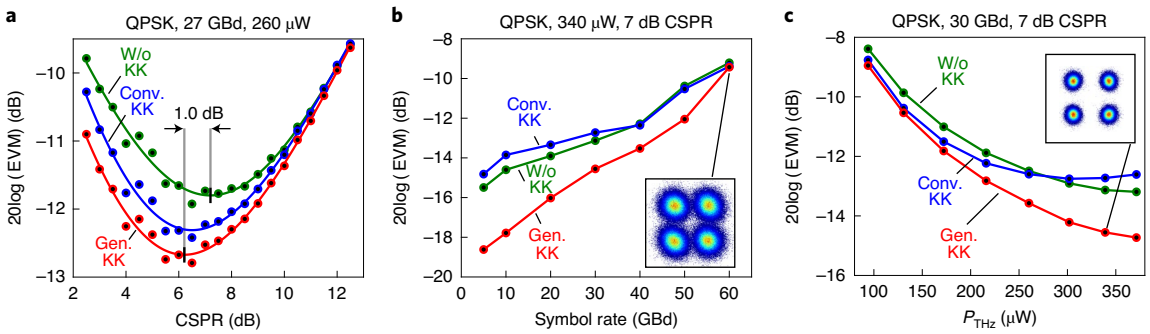

Fig. 4 | Results of the QPSK transmission experiments bridging a distance of 110 m. a, EVM as a function of the CSPR for QPSK signals measured at a symbol rate of 27 GBd for constant terahertz power $P_{THz}=260\,\mu W$. For generalized KK processing ('Gen. KK', red), the actual SBD receiver characteristics are taken into account and are compensated (equations (6) and (7)), leading to the best transmission performance. As a reference, we consider conventional KK reception ('Conv. KK', blue), assuming a quadratic relationship between the SBD current and $|\underline{U}|$, as well as heterodyne reception without any KK processing and without a guard band between the signal and the LO ('W/o KK', green), which suffers from impairments due to nonlinear interaction of the signal with itself. For all processing schemes, an optimum CSPR of around 6–7 dB is found, representing an ideal trade-off between low signal power at high CSPR and low LO power at small CSPR. The generalized KK processing shows a 1.0 dB reduction of the optimum CSPR compared with heterodyne reception without KK processing. **b**, EVM as a function of the symbol rate for a CSPR of 7 dB and $P_{THz}=340\,\mu W$. The inset shows the constellation diagram for a symbol rate of 60 GBd, for which an EVM of −9.4 dB is recorded. **c**, EVM as a function of P_{THz} for a symbol rate of 30 GBd and a CSPR of 7 dB. The performance advantages of generalized KK processing are most pronounced at high terahertz powers, where the SBD receiver characteristics cannot be approximated by a square-root relationship. An exemplary constellation diagram for a 30 GBd QPSK signal is shown in the inset.

For larger CSPRs and constant overall terahertz power P_{THz}, the data signal becomes weaker and is finally dominated by receiver noise.

Next, we evaluate the EVM for various symbol rates of up to 60 GBd at $P_{THz}=340\,\mu W$ and for a CSPR of 7 dB (Fig. 4b). For lower symbol rates, generalized KK processing clearly improves the signal quality. At higher symbol rates, thermal noise and quantization noise are the dominant limitations, and the three processing schemes converge in their performance. The inset of Fig. 4b shows the constellation diagram for the 60 GBd transmission, for which an EVM of −9.4 dB is measured. For this case, the bit error probability could be reliably estimated by measuring the BER. The BER of 1.9×10^{-3} is below the threshold of 4.4×10^{-3} for forward error correction (FEC) with 7% overhead[31] and leads to a net data rate of 112 Gbit s^{-1}.

In a third measurement, we investigate the dependence of the EVM on the incident terahertz power for a symbol rate of 30 GBd and a CSPR of 7 dB (Fig. 4c). For small terahertz powers, where the SBD characteristics can be approximated by a square-root relationship, the performance of generalized KK processing is similar to that of the conventional KK scheme. In this regime, KK processing does not show a strong advantage over heterodyne reception, because the unwanted interaction products of the signal with itself

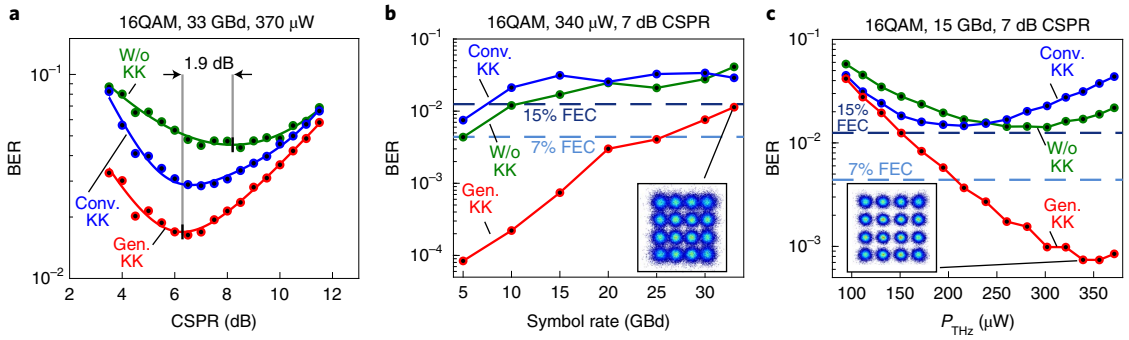

Fig. 5 | Results of the 16QAM transmission experiments bridging a distance of 110 m. a, BER as a function of the CSPR for 16QAM transmission at a symbol rate of 33 GBd at a terahertz power $P_{THz} = 370\,\mu W$. The CSPR analysis compares generalized KK processing ('Gen. KK'), conventional KK reception ('Conv. KK'), and heterodyne detection without any KK processing ('W/o KK') and exhibits similar behaviour to that for QPSK (Fig. 4a). Here also, the generalized KK processing shows a slight reduction of the optimum CSPR with respect to heterodyne reception without KK processing. This reduction amounts to 1.9 dB. **b**, BER as a function of the symbol rate at a CSPR of 7 dB and a terahertz power $P_{THz} = 340\,\mu W$. Employing generalized KK reception, the BER stays below the 15% FEC limit and leads to a line rate of 132 Gbit s^{-1} and a net data rate of 115 Gbit s^{-1} when accounting for FEC overhead. The inset shows a constellation diagram for a symbol rate of 33 GBd. **c**, BER as a function of the terahertz power P_{THz} for a symbol rate of 15 GBd and a CSPR of 7 dB. For high terahertz powers, generalized KK processing allows the BER to be reduced by more than an order of magnitude. This leads to clearly distinguishable constellation points as shown in the inset.

are comparable to or even smaller than the receiver noise power. At large terahertz powers, we observe an improvement in the EVM from −12.6 dB obtained from conventional KK processing to −14.7 dB for the generalized KK scheme. Assuming that the signal impairments can be modelled as additive white Gaussian noise, this would correspond to a BER improvement[29,30] from 1×10^{-5} to 3×10^{-8}.

The same set of measurements is repeated with 16QAM signalling, that is, at double the spectral efficiency. In these experiments, we were able to directly measure the BER for a sequence of 1.6×10^{5} received symbols. For better comparison with the QPSK results, we also show the EVM evaluation in Supplementary Section 9. The CSPR analysis (Fig. 5a) exhibits a behaviour similar to that for QPSK. In both cases, the generalized KK processing shows a slight reduction of the optimum CSPR compared with heterodyne reception without KK processing. This reduction amounts to 1.0 dB for QPSK and to 1.9 dB for 16QAM and is less pronounced than usually observed in optical communications[32]. Note that a direct comparison of our generalized terahertz KK receiver with its conventional optical counterpart is difficult—the underlying nonlinearity in our experiment has pronounced third- and fourth-order contributions, whereas an optical receiver exhibits a nearly perfect quadratic characteristic. This leads to different spectral shapes of the signal–signal mixing products and hence to different CSPR-dependent impairments.

The evaluation of the BER for various symbol rates at a terahertz power $P_{THz} = 340\,\mu W$ and a CSPR of 7 dB is shown in Fig. 5b. When using heterodyne reception without KK processing, the BER is larger than the FEC limit for 7% overhead, even for symbol rates as small as 10 GBd. Conventional KK processing does not noticeably improve the BER, because higher-order mixing products of the SBD have strong impact for the comparatively high terahertz power of 340 μW. In contrast to this, generalized KK processing allows for substantial improvement of the BER, achieving a reduction of more than an order of magnitude for small symbol rates. For higher symbol rates, thermal noise again limits the performance of the reception, reducing the performance advantage of generalized KK processing. Nevertheless, for a 16QAM symbol rate of 33 GBd and generalized KK processing, the BER is still below the 15% FEC limit[33] of 1.25×10^{-2}. This leads to a line rate of 132 Gbit s^{-1} before FEC and to a net data rate of 115 Gbit s^{-1}, which represents the highest data rate so far demonstrated for wireless terahertz transmission over distances of more than 100 m.

Finally, we investigate the dependence of the BER on the incident terahertz power for a symbol rate of 15 GBd and a CSPR of 7 dB (Fig. 5c). We find that generalized KK processing leads to a clear performance advantage over a wide range of incident terahertz powers. This demonstrates the capability of our approach, especially if phase-noise-sensitive spectrally efficient QAM formats are used.

Note that the 16QAM net data rate of 115 Gbit s^{-1} is even slightly larger than the 112 Gbit s^{-1} achieved for QPSK. This result may seem counterintuitive at first glance: by going from QPSK (2 bit per symbol) to 16QAM (4 bit per symbol), the symbol rate and hence the analogue signal bandwidth can be reduced by a factor of two, which improves the signal-to-noise ratio (SNR) by 3 dB, assuming a spectrally white noise floor. At the same time, the reduced spacing of the 16QAM constellation points increases the SNR requirement[34] by more than 6 dB. Hence, for a communication channel without bandwidth limitations, the overall transmission performance for QPSK should be better than that for 16QAM. In our case, however, the channel is bandwidth-limited by the baseband circuitry at the SBD output, which deteriorates the QPSK signal at high symbol rates, but which does not affect the less broadband 16QAM signal. We believe that the improved spectral efficiency of 16QAM will become important in view of future regulations of the terahertz spectrum[35], which will require more efficient use of this scarce resource. We therefore also tested 32QAM transmission, leading to a smaller data rate than 16QAM, which is well in line with the expectations based on the high SNR requirements[34] (Supplementary Section 7). Still, we observe clear performance advantages of the generalized KK scheme compared with its conventional counterpart. In the future, 32QAM transmission might benefit from advances in terahertz amplifier technology, leading to higher saturation output powers and lower noise figures.

In summary, we have demonstrated a greatly simplified coherent receiver scheme for terahertz data signals, combining an SBD as a simple envelope detector with generalized KK signal processing. Our scheme accounts for the real characteristics of the SBD and leads to a substantial performance improvement compared with conventional square-root KK processing or with heterodyne reception without guard band. We demonstrate the viability of the scheme using QPSK, 16QAM, and 32QAM signalling, and achieve line rates of up to 132 Gbit s^{-1}, which correspond to net data rates of up to 115 Gbit s^{-1} when accounting for the overhead of FEC. We believe that the technical simplicity of the presented KK receiver is

a unique advantage, which, in combination with further advances of terahertz technology, may be key to making terahertz communication systems a viable option for future high-capacity wireless infrastructures.

Online content

Any methods, additional references, Nature Research reporting summaries, source data, extended data, supplementary information, acknowledgements, peer review information; details of author contributions and competing interests; and statements of data and code availability are available at https://doi.org/10.1038/s41566-020-0675-0.

Received: 19 June 2019; Accepted: 8 July 2020;
Published online: 7 September 2020

References

1. Mecozzi, A., Antonelli, C. & Shtaif, M. Kramers–Kronig coherent receiver. *Optica* **3**, 1220–1227 (2016).
2. Zhong, K., Lu, C., Pak, A. & Lau, T. Digital signal processing for short-reach optical communications: a review of current technologies and future trends. *J. Lightwave Technol.* **36**, 377–400 (2018).
3. Chen, X. et al. Kramers–Kronig receivers for 100 km datacenter interconnects. *J. Lightwave Technol.* **36**, 79–89 (2018).
4. Voelcker, H. Demodulation of single-sideband signals via envelope detection. *IEEE Trans. Commun.* **14**, 22–30 (1966).
5. Kramers, M. H. A. La diffusion de la lumière par les atomes. *Atti Cong. Intern. Fis.* **2**, 545–557 (1927).
6. Kronig, R. de L. On the theory of the dispersion of X-rays. *J. Opt. Soc. Am.* **12**, 547–557 (1926).
7. Nagatsuma, T., Ducournau, G. & Renaud, C. C. Advances in terahertz communications accelerated by photonics. *Nat. Photon.* **10**, 371–379 (2016).
8. Ma, J. et al. Security and eavesdropping in terahertz wireless links. *Nature* **563**, 89–93 (2018).
9. Kawanishi, T. THz and photonic seamless communications. *J. Lightwave Technol.* **37**, 1671–1679 (2019).
10. Koenig, S. et al. Wireless sub-THz communication system with high data rate. *Nat. Photon.* **7**, 977–981 (2013).
11. Puerta, R. et al. Single-carrier dual-polarization 328 Gb/s wireless transmission in a D-band millimeter wave 2×2 MU-MIMO radio-over-fiber system. *J. Lightwave Technol.* **36**, 587–593 (2018).
12. Li, X. et al. 1 Tb/s millimeter-wave signal wireless delivery at D-band. *J. Lightwave Technol.* **37**, 196–204 (2019).
13. Seeds, A. J., Shams, H., Fice, M. J. & Renaud, C. C. Terahertz photonics for wireless communications. *J. Lightwave Technol.* **33**, 579–587 (2015).
14. Yu, X. et al. 160 Gbit/s photonics wireless transmission in the 300–500 GHz band. *APL Photon.* **1**, 081301 (2016).
15. Kallfass, I. et al. 64 Gbit/s transmission over 850 m fixed wireless link at 240 GHz carrier frequency. *J. Infrared Millim. Terahertz Waves* **36**, 221–233 (2015).
16. Ma, J., Shrestha, R., Moeller, L. & Mittleman, D. M. Invited article: channel performance for indoor and outdoor terahertz wireless links. *APL Photon.* **3**, 051601 (2018).
17. Schneider, G. J., Murakowski, J. A., Schuetz, C. A., Shi, S. & Prather, D. W. Radiofrequency signal-generation system with over seven octaves of continuous tuning. *Nat. Photon.* **7**, 118–122 (2013).
18. Carpintero, G. et al. Wireless data transmission at terahertz carrier waves generated from a hybrid InP-polymer dual tunable DBR laser photonic integrated circuit. *Sci. Rep.* **8**, 3018 (2018).
19. Nagatsuma, T. & Carpintero, G. Recent progress and future prospect of photonics-enabled terahertz communications research. *IEICE Trans. Electron.* **E98.C**, 1060–1070 (2015).
20. Harter, T. et al. 110 m THz wireless transmission at 100 Gbit/s using a Kramers–Kronig Schottky barrier diode receiver. In *Proc. 2018 European Conference on Optical Communication* 1–3 (IEEE, 2018).
21. Rappaport, T. S. et al. Millimeter wave mobile communications for 5G cellular: it will work! *IEEE Access* **1**, 335–349 (2013).
22. Andrews, J. G. et al. What will 5G be? *IEEE J. Sel. Areas Commun.* **32**, 1065–1082 (2014).
23. *Minimum Requirements Related to Technical Performance for IMT-2020 Radio Interface(s)* Report No. M.2410-0 (ITU-R, 2017).
24. Latva-aho, M. & Leppänen, K. (eds) *Key Drivers and Research Challenges for 6G Ubiquitous Wireless Intelligence* (6G Flagship, Univ. Oulu, 2019).
25. Lowery, A. J., Wang, T. & Corcoran, B. Clipping-enhanced Kramers–Kronig receivers. In *Proc. 2019 Optical Fiber Communications Conference and Exhibition* M1H.2 (OSA, 2019).
26. Ito, H., Furuta, T., Muramoto, Y., Ito, T. & Ishibashi, T. Photonic millimetre- and sub-millimetre-wave generation using J-band rectangular-waveguide-output uni-travelling-carrier photodiode module. *Electron. Lett.* **42**, 1424–1425 (2006).
27. Shoji, Y., Hamaguchi, K. & Ogawa, H. Millimeter-wave remote self-heterodyne system for extremely stable and low-cost broad-band signal transmission. *IEEE Trans. Microw. Theory Tech.* **50**, 1458–1468 (2002).
28. Hermelo, M. F. et al. Spectral efficient 64-QAM-OFDM terahertz communication link. *Opt. Express* **25**, 19360–19370 (2017).
29. Schmogrow, R. et al. Error vector magnitude as a performance measure for advanced modulation formats. *IEEE Photon. Technol. Lett.* **24**, 61–63 (2012).
30. Schmogrow, R. et al. Corrections to 'error vector magnitude as a performance measure for advanced modulation formats'. *IEEE Photon. Technol. Lett.* **24**, 2198 (2012).
31. Smith, B. P., Farhood, A., Hunt, A., Kschischang, F. R. & Lodge, J. Staircase codes: FEC for 100 Gb/s OTN. *J. Lightwave Technol.* **30**, 110–117 (2012).
32. Li, Z. et al. Digital linearization of direct-detection transceivers for spectrally efficient 100 Gb/s/λ WDM metro networking. *J. Lightwave Technol.* **36**, 27–36 (2018).
33. Cai, Y. et al. FPGA investigation on error-floor performance of a concatenated staircase and Hamming code for 400G-ZR forward error correction. *J. Lightwave Technol.* **37**, 188–195 (2019).
34. Essiambre, R.-J. et al. Capacity limits of optical fiber networks. *J. Lightwave Technol.* **28**, 662–701 (2010).
35. *IEEE Standard for High Data Rate Wireless Multi-Media Networks—Amendment 2: 100 Gb/s Wireless Switched Point-to-Point Physical Layer* Standard No. 802.15.3d-2017 (IEEE, 2017).

Methods

SBD. We use a zero-bias SBD[36,37] (Virginia Diodes, WR3.4ZBD-F) as a terahertz envelope detector. This device offers high responsivity of the order of 2,000 V W^{-1} along with broadband output circuitry (bandwidth approximately 40 GHz) for down-conversion of high-speed data signals. The rectangular waveguide input port (WR 3.4) of the SBD allows us to directly connect the device to the output of a terahertz low-noise amplifier[38], designed for operation in the submillimetre H-band (0.220–0.325 THz) (Supplementary Section 4).

Phase reconstruction by KK processing. On a fundamental level, KK processing[1] relies on data signals that are analytic. For an arbitrary analytic time-domain signal $\underline{s}(t) = s_r(t) + js_i(t)$, the imaginary part $s_i(t)$ and the real part $s_r(t)$ are connected by a Hilbert transform:

$$s_i(t) = \frac{1}{\pi}\mathcal{P}\int_{-\infty}^{\infty}\frac{s_r(\tau)}{t-\tau}\mathrm{d}\tau = \mathcal{P}\left\{\frac{1}{\pi t} * s_r(t)\right\}, \tag{9}$$

$$s_r(t) = -\frac{1}{\pi}\mathcal{P}\int_{-\infty}^{\infty}\frac{s_i(\tau)}{t-\tau}\mathrm{d}\tau = -\mathcal{P}\left\{\frac{1}{\pi t} * s_i(t)\right\}, \tag{10}$$

where the asterisks denote a convolution. Equations (9) and (10) can be interpreted as the time-domain analogue of the KK relations[5,6] that connect the real and the imaginary part of a transfer function belonging to a system that is causal in the time domain[39].

Analytic signals as defined by equations (9) and (10) feature single-sided power spectra, which do not contain any spectral components for negative frequencies $\omega < 0$. Note that the mutual relationships between the imaginary and the real part of an analytic signal are defined only if both the real and the imaginary part are zero mean. To understand this, let us consider a signal with real part $s'_r(t) = s_r(t) + C_r$ that consists of a constant d.c. part C_r and a zero-mean signal $s_r(t)$. When introducing $s'_r(t)$ into equation (9), the integral has to be evaluated in the sense of a Cauchy principal value to ensure convergence both for the singularity at $t=\tau$ and for the infinite integration limits

$$s_i(t) = \frac{1}{\pi}\lim_{\varepsilon\to 0}\left(\int_{t-1/\varepsilon}^{t-\varepsilon}\frac{s'_r(\tau)}{t-\tau}\mathrm{d}\tau + \int_{t+\varepsilon}^{t+1/\varepsilon}\frac{s'_r(\tau)}{t-\tau}\mathrm{d}\tau\right). \tag{11}$$

In this case, the constant C_r does not contribute to $s_i(t)$, and when using equation (10) to reconstruct the real part, we would obtain $s_r(t)$ rather than $s'_r(t)$. Similarly, using equation (10) to reconstruct $s_r(t)$ from an imaginary part $s'_i(t) = s_i(t) + C_i$ with non-zero mean value C_i would suppress the constant d.c. part C_i and produce the real part $s_r(t)$ that belongs to the corresponding zero-mean signal $s_i(t)$. Hence, signals with non-zero mean value, that is, non-zero spectral power at frequency $f=0$, are not analytic signals in the sense of equations (9) and (10).

For KK-based transmission, the analytic data signal $\underline{U}_s(t)$ is superimposed with a carrier tone, represented by a constant voltage U_0 in the baseband. Without loss of generality, we assume U_0 to be real-valued and positive. The overall complex envelope can then be written as

$$\underline{U}(t) = U_0 + \underline{U}_s(t) = |\underline{U}(t)|\mathrm{e}^{j\Phi(t)}. \tag{12}$$

In technical implementations of KK reception, $|\underline{U}(t)|$ can be directly measured through some sort of envelope detector with nonlinear characteristics such as a photodiode or, as in our case, an SBD. To establish a relation between the amplitude $|\underline{U}(t)|$ and the phase $\Phi(t)$ of the complex envelope $\underline{U}(t)$, we derive an auxiliary signal $\underline{s}(t)$ by applying the complex natural logarithm to equation (12):

$$\underline{s}(t) = \ln(\underline{U}(t)) = \ln(|\underline{U}(t)|) + j\Phi(t). \tag{13}$$

For our further analysis, we exploit the fact that $\underline{s}(t)$ is an analytic signal if the complex data signal $\underline{U}_s(t)$ is an analytic signal too and if, in addition, $\underline{U}(t)$ is minimum phase[1]. A necessary condition for $\underline{U}(t)$ being minimum phase is that the associated time-dependent trajectory described by $\underline{U}(t)$ in the complex plane does not encircle the origin, which is ensured if $|\underline{U}_s(t)| < U_0\ \forall t$. In this case, we may apply equation (9) to the auxiliary analytic signal $\underline{s}(t)$ and obtain

$$\Phi(t) = \frac{1}{\pi}\mathcal{P}\int_{-\infty}^{\infty}\frac{\ln(|\underline{U}(\tau)|)}{t-\tau}\mathrm{d}\tau. \tag{14}$$

This relation allows us to reconstruct the phase of $\underline{U}(t)$ if only the magnitude $|\underline{U}(t)|$ is known. The complex data signal $\underline{U}_s(t) = |\underline{U}_s(t)|\exp(j\varphi_s(t))$ with magnitude $|\underline{U}_s(t)|$ and phase φ_s is then recovered from $\underline{U}(t)$ by subtracting the constant d.c. voltage U_0 corresponding to the amplitude of the carrier tone, see equation (12)

$$\underline{U}_s(t) = |\underline{U}_s(t)|\mathrm{e}^{j\varphi_s(t)} = |\underline{U}(t)|\mathrm{e}^{j\varphi(t)} - U_0. \tag{15}$$

Note that the voltage magnitude in equation (14) can be scaled with an arbitrary constant factor ζ without changing the reconstructed $\Phi(t)$. This becomes plausible when considering that $\ln(\zeta|\underline{U}(t)|) = \ln(|\underline{U}(t)|) + \ln(\zeta)$ and that the constant $\ln(\zeta)$ is suppressed when applying the Hilbert transform according to equation (14), see the discussion after equation (11).

Heterodyne reception without guard band. In our evaluation, we also consider single-ended heterodyne reception without any KK processing, which does not account for nonlinear interaction of the signal with itself. According to equation (5), $i(t)$ depends on the magnitude of $|\underline{U}(t)|$. For the sake of simplicity, we assume a square-law relationship $i(t) \propto |\underline{U}(t)|^2$ in the following derivation. With equation (2), we obtain

$$i(t) \propto |U_0 + \underline{U}_s(t)|^2 = U_0^2 + |\underline{U}_s(t)|^2 + 2U_0\Re(\underline{U}_s(t)). \tag{16}$$

The component $2U_0\Re\{\underline{U}_s(t)\}$ corresponds to the mixing product of the LO tone with amplitude U_0 and the analytic data signal $\underline{U}_s(t)$ and allows us to recover the data signal. However, there is also the mixing product $|\underline{U}_s(t)|^2$ of the signal with itself, which covers the same spectral region as $2U_0\Re\{\underline{U}_s(t)\}$, unless a guard band between U_0 and the data spectrum is used. This mixing product degrades the received signal quality and can be compensated by using KK processing, as described in the main text. For large CSPRs, that is, large values of U_0, the data can still be recovered without using KK processing, because the data signal $2U_0\Re(\underline{U}_s(t))$ dominates over the unwanted mixing product for $|U_0| \gg |U_s(t)|$. In Supplementary Section 8, we compare the generalized KK scheme to heterodyne detection with a guard band and find that both schemes offer similar transmission performances, while the generalized KK scheme overcomes the need for a guard band.

DSP chain. In our experiments, we digitize the receiver currents using a real-time oscilloscope (Keysight UXR0804A) and store the recorded waveforms for subsequent offline DSP and signal-quality evaluation. The transmitted data signal $|\underline{U}_s(t)|\exp(j\varphi_s(t))$ is reconstructed from the digitally captured SBD current by generalized KK processing (equations (5) and (6)). We first calculate $|\underline{U}(t)|$ from the captured signal by inverting equation (5). For the phase reconstruction (equation (6)), the Hilbert transform is implemented as a convolution with a discrete-time finite-impulse-response filter[40]. For the processing, an oversampling of six samples per symbol is used to avoid performance penalties due to spectral broadening[41] introduced by the natural logarithm in equation (6) and by the function in equation (7). Note that the rather large oversampling was chosen to guarantee optimum performance in the proof-of-principle demonstration. The system, however, performs equally well for a sampling with only three samples per symbol (Supplementary Section 6). After phase reconstruction, the complex signal $\underline{U}(t)$ is down-sampled to a ratio of two samples per symbol, and the analytic signal $\underline{U}_s(t)$ is obtained according to equation (15). The original QAM signal is then recovered by down-converting $\underline{U}_s(t)$ to the baseband. The KK receiver DSP is followed by the DSP blocks of a fully blind coherent optical receiver[42], with the exception that only a single polarization is evaluated. Specifically, we perform a timing-error estimation in the frequency domain, followed by a compensation with a Lagrange interpolator in a Farrow[43] structure. We then apply an adaptive feed-forward equalizer, whose coefficients are adapted blindly using the constant-modulus algorithm[44]. The remaining frequency offset originating from frequency drifts of the LO laser at f_1 as well as of the signal laser at f_0 is removed, and a subsequent phase recovery using the blind phase search algorithm[45] combats laser phase noise. Finally, we apply a real-valued multiple-input multiple-output feed-forward equalizer with the in-phase (I) and the quadrature (Q) components of the complex baseband as individual inputs to compensate IQ imbalances of the transmitter hardware[46]. The feed-forward equalizer coefficients are adapted by a decision-directed least-mean-square algorithm[47]. Eventually, the BER and EVM are calculated. Compared with conventional terahertz receiver concepts, the KK scheme comes at the cost of extra DSP for the phase reconstruction. However, the outputs of the DSP blocks containing $g^{-1}(i)$ and the natural logarithm in equation (6) as well as the complex exponential in equation (2) can be stored in look-up tables. Furthermore, the Hilbert transform can be implemented without considerable performance degradation[40] by a convolution of the reconstructed $|\underline{U}(t)|$ with a discrete-time finite-impulse-response filter that has only a small number of taps. By considering an advanced implementation of the KK processing that works at a reduced oversampling ratio of two samples per symbol, the DSP complexity can be reduced even further[48,49]. The overall DSP effort, also including steps such as timing recovery, phase estimation and FEC, will hence not be substantially increased by KK-type phase reconstruction. We therefore believe that the additional KK-related DSP complexity will be overcompensated by the reduced hardware complexity.

EVM and BER. The EVM and BER are standard metrics to evaluate the quality of communication signals and are widely used in the optical and terahertz communications community[29,30]. Assuming data-aided reception of N randomly transmitted symbols, the EVM is a measure for the effective distance of the received complex symbols $\underline{E}_r$ from their ideal positions $\underline{E}_t$ in the constellation

diagram. Specifically, it relates the root-mean-square value σ_{err} of the error vector amplitude $|\underline{E}_{\mathrm{r}} - \underline{E}_{\mathrm{t}}|$ to the root-mean-square value $|\underline{E}_{\mathrm{t,a}}|$ of the N ideal constellation points

$$\mathrm{EVM} = \frac{\sigma_{\mathrm{err}}}{|\underline{E}_{\mathrm{t,a}}|},$$

$$\mathrm{EVM}_{\mathrm{dB}} = 20\log(\mathrm{EVM}),$$

$$|\underline{E}_{\mathrm{t,a}}|^2 = \frac{1}{N}\sum_{n=1}^{N}|\underline{E}_{\mathrm{t},n}|^2,$$

$$\sigma_{\mathrm{err}}^2 = \frac{1}{N}\sum_{n=1}^{N}|\underline{E}_{\mathrm{r},n} - \underline{E}_{\mathrm{t},n}|^2,$$

In these relations, $\mathrm{EVM}_{\mathrm{dB}}$ is the EVM expressed in decibels, $\underline{E}_{\mathrm{t},n}$, and $\underline{E}_{\mathrm{r},n}$ $n = 1 \ldots N$ correspond to the complex amplitudes of the ideal transmitted and the real received symbols, and $|\underline{E}_{\mathrm{t,a}}|^2$ corresponds to the average power of the signal. The BER is obtained by comparing the digitally processed bit sequence with the known transmitter bit sequence and by relating the number of counted errors to the total number of bits. For the results shown in Figs. 4 and 5, a random pattern of length 2^{15} (QPSK) or 2^{14} (16QAM) symbols is periodically repeated. The real-time oscilloscope records a sequence of 8×10^6 samples at a sampling rate of 128 GSa s^{-1} ('Sa' stands for samples) for symbol rates smaller than 20 GBd, and at a sampling rate of 256 GSa s^{-1} for symbol rates ≥20 GBd. These correspond to recording lengths of 31.25 µs and 62.50 µs, respectively. The BER and EVM evaluation is restricted to the last ten transmit pattern periods to ensure that the equalizers have already converged. In the case of QPSK modulation, the signal quality is so good that only very few errors can be found for the given recording length. Generally, if fewer than 13 errors are counted in a recording, the measured BER is not a reliable estimate[50] of the actual bit error probability due to poor statistics. Moreover, since the constellation points seen in Figs. 4 and 5 are not perfectly circular, the assumption of additive white Gaussian noise is violated, and we refrain from estimating the BER from the EVM. Therefore, the measured EVM itself is used as a quality metric for QPSK signals.

Data availability

The data that support the findings of this study are available from the corresponding author on reasonable request.

References

36. Hesler, J., Hui, K. & Crowe, T. Ultrafast millimeter wave and THz envelope detectors for wireless communications. In *Proc. 2012 International Topical Meeting on Microwave Photonics* 93–94 (IEEE, 2012).
37. Hesler, J. L. & Crowe, T. W. NEP and responsivity of THz zero-bias Schottky diode detectors. In *Proc. Joint 32nd International Conference on Infrared and Millimeter Waves and 15th International Conference on Terahertz Electronics* 844–845 (IEEE, 2007).
38. Tessmann, A. et al. High-gain submillimeter-wave mHEMT amplifier MMICs. In *Proc. 2010 MTT-S International Microwave Symposium* 53–56 (IEEE, 2010).
39. Toll, J. S. Causality and the dispersion relation: logical foundations. *Phys. Rev.* **104**, 1760–1770 (1956).
40. Füllner, C. et al. Complexity analysis of the Kramers–Kronig receiver. *J. Lightwave Technol.* **37**, 4295–4307 (2019).
41. Li, Z. et al. Joint optimisation of resampling rate and carrier-to-signal power ratio in direct-detection Kramers–Kronig receivers. In *Proc. 2017 European Conference on Optical Communication* W2D.3 (IEEE, 2017).
42. Savory, S. J. Digital coherent optical receivers: algorithms and subsystems. *IEEE J. Sel. Top. Quantum Electron.* **16**, 1164–1179 (2010).
43. Farrow, C. W. A continuously variable digital delay element. In *Proc. 1988 International Symposium on Circuits and Systems* 2641–2645 (IEEE, 1988).
44. Godard, D. N. Self-recovering equalization and carrier tracking in two-dimensional data communication system. *IEEE Trans. Commun.* **28**, 1867–1875 (1980).
45. Pfau, T. & Hoffmann, S. Hardware-efficient coherent digital receiver concept with feedforward carrier recovery for M-QAM constellations. *J. Lightwave Technol.* **27**, 989–999 (2009).
46. Randel, S. et al. All-electronic flexibly programmable 864 Gb/s single-carrier PDM-64-QAM. In *Proc. 2014 Optical Fiber Communication Conference* Th5C.8 (OSA, 2014).
47. Faruk, S. & Savory, S. J. Digital signal processing for coherent transceivers employing multilevel formats. *J. Lightwave Technol.* **35**, 1125–1141 (2017).
48. Bo, T. & Kim, H. Kramers–Kronig receiver operable without digital upsampling. *Opt. Express* **26**, 13810–13818 (2018).
49. Mecozzi, A., Antonelli, C. & Shtaif, M. Kramers–Kronig receivers. *Adv. Opt. Photon.* **11**, 480–517 (2019).
50. Freude, W. et al. Quality metrics for optical signals: eye diagram, Q-factor, OSNR, EVM and BER. In *Proc. 14th International Conference on Transparent Optical Networks* 1–4 (IEEE, 2012).

Acknowledgements

This work was supported by the European Research Council (ERC consolidator grant 'TeraSHAPE', no. 773248), the Alfried Krupp von Bohlen und Halbach Foundation, the Helmholtz International Research School of Teratronics (HIRST) and the Karlsruhe School of Optics and Photonics (KSOP). The work relies on instrumentation funded by the European Regional Development Fund (ERDF, grant EFRE/FEIH_776267), the Deutsche Forschungsgemeinschaft (DFG; grants DFG/INST 121384/166-1 and DFG/INST 121384/167-1) and the Hector Stiftung (Hector Foundation).

Author contributions

T.H., C.F. and C.K. developed the idea; J.L.H. developed and supplied the SBD; the experiments were performed by T.H. and C.F. with the support of J.N.K., S.U., J.L.S., M.B. and E.B.; algorithms for data generation and signal processing were implemented by T.H., C.F. and S.R.; the project was supervised by A.-S.M., W.F., S.R. and C.K.; the paper was written by T.H., C.F., W.F., S.R. and C.K.; all authors revised the paper.

Competing interests

J.L.H. is chief technology officer of Virginia Diodes Inc., a company manufacturing and selling high-speed SBDs for terahertz signal processing. All other authors have no competing interests.

Additional information

Supplementary information is available for this paper at https://doi.org/10.1038/s41566-020-0675-0.

Correspondence and requests for materials should be addressed to C.K.